Vectorial magnetometry with the magneto-optic Kerr effect applied to Co/Cu/Co trilayer structures

C. Daboo, J. A. C. Bland, R. J. Hicken, A. J. R. Ives, and M. J. Baird
Cavendish Laboratory, University of Cambridge, Madingley Road, Cambridge CB3 0HE, United Kingdom

M. J. Walker
Condensed Matter Physics Group, Department of Physics, University of Leeds, Leeds LS2 9JT, United Kingdom
(Received 28 September 1992)

We describe an arrangement in which the magnetization components parallel and perpendicular to the applied field are both determined from longitudinal magneto-optic Kerr effect measurements. This arrangement differs from the usual procedures in that the same *optical* geometry is used but the *magnet* geometry altered. This leads to two magneto-optic signals which are directly comparable in magnitude thereby giving the in-plane magnetization vector directly. We show that it is of great value to study both in-plane magnetization vector components when studying coupled structures where significant anisotropies are also present. We discuss simulations which show that it is possible to accurately determine the coupling strength in such structures by examining the behavior of the component of magnetization perpendicular to the applied field in the vicinity of the hard in-plane anisotropy axis. We illustrate this technique by examining the magnetization and magnetic anisotropy behavior of ultrathin Co/Cu(111)/Co (d_{Cu}=20 Å and 27 Å) trilayer structures prepared by molecular beam epitaxy, in which coherent rotation of the magnetization vector is observed when the magnetic field B is applied along the hard in-plane anisotropy axis, with the magnitude of the magnetization vector constant and close to its bulk value. Results of micromagnetic calculations closely reproduce the observed parallel and perpendicular magnetization loops, and yield strong uniaxial magnetic anisotropies in both layers, while the interlayer coupling appears to be absent or negligible in comparison with the anisotropy strengths.

I. INTRODUCTION

Measurement of the magnetization curve is important in gaining an understanding of the magnetic behavior of ultrathin-film structures, providing valuable information on magnetic anisotropies and the mechanism for magnetization reversal. Conventional magnetometric methods using, for example, vibrating sample magnetometry, superconducting quantum interference device susceptometry and magnetization loopers, or the magneto-optic Kerr effect (MOKE) are often used to determine a single component of the magnetization, usually parallel to the applied field. However, a better understanding of the in-plane magnetization reversal process can be gained by adapting these techniques to measure two perpendicular components of the magnetization, allowing a determination of the magnitude and direction of the total magnetization in-plane as a function of the applied field. Several methods for achieving this have already been described,[1] based around the MOKE technique[2,3] in particular. MOKE is of particular value in studying ultrathin films because of its high sensitivity and in this paper we show that it is possible to directly obtain the components of magnetization, normalized to the saturation value, both parallel and perpendicular to the applied field direction using MOKE.

Florczak and Dahlberg[2] describe how they use the "physical distinction" between the longitudinal and transverse Kerr effects to measure two perpendicular magnetization components in-plane. We have used a similar approach based on MOKE, but in our case we change the sample/magnet geometry, while measuring the longitudinal MOKE effect only. This has the advantage that the magnitude of the parallel and perpendicular magnetization components can be directly compared. It is also possible to observe the out-of-plane magnetization component by choosing a particular MOKE geometry.[4] Such measurements combined with the in-plane magnetization measurements allows a complete determination of the direction (in three dimensions) and relative magnitude (M/M_s) of the magnetization vector.

It is of particular value to study the layer-dependent magnetization orientation as a function of applied field in coupled films[5] exhibiting giant magnetoresistance[6,7] (GMR), since the spin orientation determines the GMR via the spin-valve effect,[8] for example. In the case of antiferromagnetic (AF) coupling, where magnetizations prefer to lie antiparallel, the total magnetization is close to zero at zero applied field in the absence of significant anisotropies, whereas for ferromagnetic (FM) coupling, where the magnetizations prefer a parallel alignment, the total magnetization is close to the sum of the individual component magnetizations. Therefore, the shape of the M-H loop, which depends on the nature of any anisotropies and coupling, gives insight into the sign of the coupling, although in the FM-coupling case it is not usually possible to estimate the strength of the coupling.

In this paper we illustrate our MOKE analysis technique by examining a coherent magnetization rotation process which we have found to occur in a Co/Cu(111)/Co/Ge system grown on a GaAs(110) sub-

strate by molecular beam epitaxy (MBE). Calculations based on both tight-binding and Ruderman-Kittel-Kasuya-Yosida models predict an oscillatory coupling period close to 10 Å for a (111) surface, and therefore we *expect* oscillatory coupling for Cu(111) spacer layers[9,10] regardless of the growth mechanism (sputtering or MBE). Recently, contradictory results have appeared for the existence of coupling in MBE-grown Co/Cu(111)/Co structures. Egelhoff and Kief[11] grew Co/Cu(111)/Co samples which apparently showed no AF coupling, whereas Johnson *et al.*[12] have seen AF coupling in such samples, though it is intermixed with ferromagnetic (FM) coupling. Johnson *et al.*[12] explain this by suggesting that there is significant pinhole formation or local thinning of the Cu interlayer, which would be less likely to occur in sputtered films where strong AF coupling has been observed. However, several groups have recently reported evidence of AF coupling and giant MR in MBE-grown (111) oriented structures.[13,14]

For samples investigated here, we find no evidence for interlayer coupling of a strength comparable to that observed in sputtered films, although we note that the occurrence of strong anisotropies which occur in our samples can mask the effect of coupling upon the shape of the *M-H* loops. However, we describe the results of simulations which show that the magnitude of the effective field associated with any AF coupling (the coupling field), if present, is very weak ($<1\%$) in comparison with the effective field associated with the anisotropy (the anisotropy field). This behavior is likely to result from the larger degree of roughness which occurs in the films we have investigated, in comparison with that occurring in similar structures grown by first preparing a seed layer of Au, for which GMR has been observed.[13] The simulations show that the component of magnetization perpendicular to the applied field is sensitively dependent on the AF coupling strength even when it is weak in comparison to the anisotropy, in contrast to the parallel component of the magnetization, which is usually investigated. This illustrates the value of performing vectorial magnetization measurements when studying interlayer coupling.

II. MOKE TECHNIQUE

The magneto-optic Kerr effect (MOKE) can be observed as a change in the intensity and/or polarization state of light reflected from a magnetized sample as a function of the applied magnetic field. The Kerr signal is induced by a specific component of the magnetization which is determined by the experimental geometry in use. Here MOKE was used to determine the relative magnitude (M/M_s) and direction of the magnetization components in the Co layers by measuring the MOKE signal caused by components of the magnetization parallel ($M_{\parallel}$) and perpendicular ($M_{\perp}$) to the applied field in the plane of the sample.

There are three common MOKE geometries that are used: the longitudinal geometry, in which the applied field lies in the plane of the sample and in the scattering plane; the transverse geometry, in which the applied field still lies in the plane of the sample but is perpendicular to the scattering plane; and the polar geometry, in which the applied field is perpendicular to the plane of the sample and in the scattering plane. It is important to distinguish between the orientation of the applied field and that of the magnetization with respect to the scattering plane.

The nature of the Kerr effect depends on the orientation of the *magnetization* with respect to the scattering plane and the plane of the sample. When the magnetization is in the longitudinal or polar orientations, the Kerr effect manifests itself as a change in the *polarization* state of the reflected light (to first order), which causes initially plane polarized light to become elliptically polarized on reflection. In the transverse orientation, the Kerr effect is seen as a change in the *intensity* of the reflected beam (for *p*-polarized incident light only), and no ellipticity occurs. This is summarized in Table I, which shows the calculated Fresnel coefficients for *p*-polarized light incident on a single interface nonmagnetic/magnetic layer system in the three standard geometries. The magneto-optic coefficients Q_P, Q_L, and Q_T are proportional to the magnitude of the component of the magnetization along the corresponding direction.

TABLE I. The Fresnel coefficients for *p*-polarized light incident on a single interface nonmagnetic/magnetic layer system. The complex dielectric constants of each layer are ε_1 and ε_2, and the angle to the normal of the interface that the light makes in each layer is given by θ_1 and θ_2. The substitutions $\alpha_1=\cos\theta_1$ and $\alpha_2=\cos\theta_2$ have been used.

	r_{pp}	r_{ps}
Polar	$\dfrac{\sqrt{\varepsilon_2}\alpha_1-\sqrt{\varepsilon_1}\alpha_2}{\sqrt{\varepsilon_2}\alpha_1+\sqrt{\varepsilon_1}\alpha_2}$	$\dfrac{Q_P\sqrt{\varepsilon_1\varepsilon_2}\alpha_1}{i(\sqrt{\varepsilon_2}\alpha_1+\sqrt{\varepsilon_1}\alpha_2)(\sqrt{\varepsilon_1}\alpha_1+\sqrt{\varepsilon_2}\alpha_2)}$
Long.	$\dfrac{\sqrt{\varepsilon_2}\alpha_1-\sqrt{\varepsilon_1}\alpha_2}{\sqrt{\varepsilon_2}\alpha_1+\sqrt{\varepsilon_1}\alpha_2}$	$\dfrac{Q_L\sqrt{\varepsilon_1\varepsilon_2}\alpha_1\tan\theta_2}{i(\sqrt{\varepsilon_2}\alpha_1+\sqrt{\varepsilon_1}\alpha_2)(\sqrt{\varepsilon_1}\alpha_1+\sqrt{\varepsilon_2}\alpha_2)}$
Trans.	$\dfrac{\sqrt{\varepsilon_2}\alpha_1\sqrt{1-Q_T^2/\alpha_2^2}-\sqrt{\varepsilon_1}\alpha_2-i\sqrt{\varepsilon_2}Q_T\alpha_1\tan\theta_2}{\sqrt{\varepsilon_2}\alpha_1\sqrt{1-Q_T^2/\alpha_2^2}+\sqrt{\varepsilon_1}\alpha_2-i\sqrt{\varepsilon_2}Q_T\alpha_1\tan\theta_2}$	0

For conventional MOKE measurements, plane polarized light is reflected from a magnetized sample and then passes through an analyzing polarizer (the analyzer) and is incident on a photodetector, providing the signal. The setting of the analyzer depends on the orientation of the component of magnetization to be detected. For the longitudinal or polar orientations the analyzer is set close to extinction (analyzer angle of 90° with respect to the incident plane of polarization) to observe a change in the polarization state. For the transverse orientation the analyzer is set to transmit light with the same polarization as the incident light (analyzer angle of 0°).

The distinction between the orientation of the applied field and the component of the magnetization being observed is of key importance. For the applied field the terms PF, LF, and TF are used for the polar, longitudinal, and transverse geometries, respectively. For the magnetization components the terms PM, LM, and TM are used to describe the orientation of the component being detected. Thus it is possible to have the magnet in the transverse geometry, while detecting the longitudinal component of the magnetization (TF/LM), for example.

Since the longitudinal magnetization component produces a change in r_{ps} only, while the transverse magnetization component produces a change in r_{pp} only (see Table I), it is possible to measure these components independently of each other, allowing a determination of components parallel and perpendicular to the applied field.

There are therefore two possible ways to measure both $M_{\parallel}$ and $M_{\perp}$: One method relies on the direction of the applied magnetic field remaining fixed, while the analyzer is rotated;[2] the other uses a fixed analyzer but the applied field and sample are rotated together (as illustrated in Fig. 1). The first method measures $M_{\parallel}$-H and $M_{\perp}$-H loops by using the longitudinal and transverse MOKE effects, respectively, so the two loops are not directly comparable in amplitude as the nature of the two optical effects involved are different in each case. The second method allows a direct comparison between the $M_{\parallel}$-H and $M_{\perp}$-H loops, since they are both measured using the same longitudinal MOKE effect. In this case the relative amplitude and direction of M can immediately be obtained.

For a system with a single magnetic layer with a magnetization of magnitude M (which may not be constant), the two MOKE loops are proportional to $M\cos\theta$ and $M\sin\theta$, where θ is the angle between the magnetization and the applied field direction. Using the two loops it is therefore possible to determine the relative magnitude and direction (with respect to the applied field) of the magnetization. For a system with two or more layer-dependent magnetizations M_i, the MOKE loops are now proportional to the sum of each component, i.e., $\sum_i M_i\cos\theta_i$ and $\sum_i M_i\sin\theta_i$. In this case it is not possible to determine the magnitude and orientations of each layer-dependent magnetization explicitly. However, the coherent rotation process can be observed by comparing the magnitude of the signal for the saturated state, i.e., $\sum_i M_i$, with the total magnitude along some direction for different field strengths. When the total magnitude is equal to the total saturation magnetization then the magnetizations of each layer are pointing in the same direction and have their full saturation magnetization value.

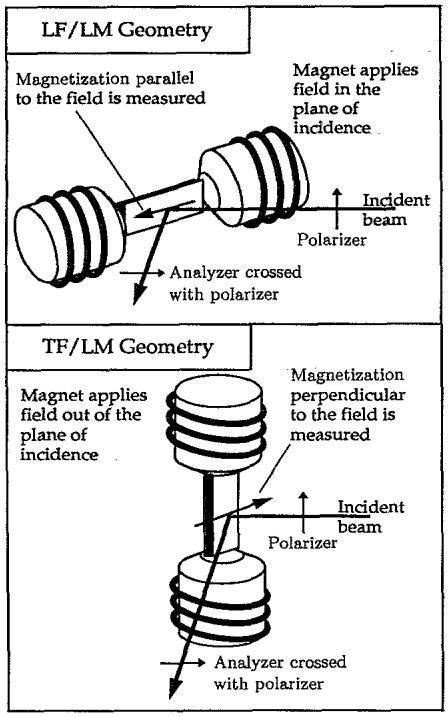

FIG. 1. An illustration of the two experimental geometries used to measure the components of magnetization parallel and perpendicular to the applied field.

III. EXPERIMENTAL DETAILS

A. Sample preparation

Two samples were grown on a GaAs (110) substrate in a VG80M molecular-beam-epitaxy facility in which the base pressure was 4.5×10^{-11} mbar. Prior to the actual growth cycle the substrate was heated to a nominal temperature of 595 °C to achieve the reflection high-energy electron-diffraction (RHEED) streaks characteristic of a (110) surface reconstruction.

A 500 Å buffer layer of germanium was then grown at a rate of about 0.16 Å/sec on top of the substrate which was held at a temperature of 500 °C. As is normal in the preparation of metallic multilayers, the Co/Cu/Co trilayers were deposited at a much lower temperature—in this case 100 °C. Both metals were evaporated from electron-beam sources with the rates of deposition being approximately 0.2 Å/sec for each. During the growth the background pressure in the growth chamber never rose higher than 2×10^{-10} mbar. From the RHEED patterns along the (110) azimuth the lower layer of cobalt was deduced to grow in the bcc (100) phase, while the copper and the upper cobalt layer were deduced to grow in the fcc (111) phase. The trilayer thicknesses were estimated to be 30 Å for both Co layers in each sample and Cu layer thicknesses of 27 Å (sample A) and 20 Å (sample

B). The samples were then capped with 120 Å of Cu. The Cu spacer layer thicknesses chosen correspond to those at which FM (sample A) and AF (sample B) coupling have been observed in *sputtered* films.[7]

B. MOKE apparatus

A conventional MOKE arrangement was used for the experiments that were made at room temperature. An intensity stabilized HeNe laser of wavelength 632.8 nm and nominal power 20 mW illuminated the sample, which was mounted between the poles of an electromagnet. The intensity stabilizer[15] consisted of an electro-optic cell, quarter-wave plate, polarizer, beamsplitter, and reference photodiode. The signal from the photodiode was fed into a differential amplifier which had an adjustable reference voltage on its other input. The resulting amplified error signal was then applied to the electro-optic cell. Careful adjustment of the parameters of the feedback loop lead to an intensity stability of better than 0.1%.

The angle of incidence of the laser beam on the sample was about 33°, and the reflected beam passed through an analyzing polarizer and then onto a photodiode. A Hall sensor was attached to one of the pole pieces of the electromagnet and calibrated so that the measured Hall voltage could be converted into the value of the field at the center of the pole pieces where the sample was located. The experiment was controlled by a computer which was used to vary the field produced by the electromagnet, while recording the Hall voltage and photodiode signal.

The sample was mounted on a rotary stage which had its axis of rotation in the plane of incidence, and was adjusted so that the reflected beam did not move as the sample stage was rotated through a full 360°. The orientation of the magnet could be changed without disturbing the sample stage so that the field could be applied in either the longitudinal or transverse geometries, depending on the component of magnetization to be measured.

IV. DISCUSSION

A. Calculations

The static orientation of the magnetization vectors in coupled trilayer films may be determined by minimizing the magnetic free energy of the system. For ultrathin films the magnetization of each layer may be assumed to be spatially uniform, in which case its orientation may be described by just two angles. In addition, if the perpendicular anisotropy energy, which includes both volume and surface contributions, is small relative to the demagnetizing energy or at least favors in-plane magnetization, then the magnetization of each layer may be assumed to be confined to the film plane. Assuming that the above conditions are satisfied, only one angle is required to describe the orientation of the magnetization in a layer and so minimization of the free energy is performed with respect to just two variables.

The coupling energy between the magnetic layers is usually assumed to give rise to a surface energy density of the form

$$E_s = -2A_{12}\hat{\mathbf{M}}_1\cdot\hat{\mathbf{M}}_2 , \tag{1}$$

where $\hat{\mathbf{M}}_1$ and $\hat{\mathbf{M}}_2$ are unit vectors in the direction of the magnetizations of the two layers, and A_{12} is the coupling constant which depends on the thickness of the spacer layer. We note that higher order terms in $\hat{\mathbf{M}}_1\cdot\hat{\mathbf{M}}_2$, such as the biquadratic coupling term, which has been both observed[16] and explained by means of a fluctuation mechanism,[17] may easily be included in the above expression if necessary. If E_1 and E_2 are the volume energy densities of the two layers in the absence of coupling then the total magnetic energy of the system may be written as

$$E = A(d_1E_1 + d_2E_2 - 2A_{12}\hat{\mathbf{M}}_1\cdot\hat{\mathbf{M}}_2) , \tag{2}$$

where A is the surface area of the film and d_1 and d_2 are the thicknesses of the two layers. In general E_1 and E_2 will include Zeeman and anisotropy energy density terms; the latter is the sum of the magnetocrystalline anisotropy, which depends upon the structure and orientation of the magnetic layer, strain-induced anisotropies, which have been observed in ultrathin bcc Co films,[18,19] and anisotropies due to defects such as steps.[20,21] For the Co/Cu/Co samples discussed in this paper we find it is sufficient to include only a uniaxial anisotropy term so that we have

$$E_i = K_i\cos^2\theta_i - M_iH\cos(\theta_i - \theta_H) , \tag{3}$$

where K_i is the volume uniaxial anisotropy constant, H is the applied magnetic field strength, M_i is the magnetization, and θ_i and θ_H are the angles defining the orientation of the magnetization and applied field, respectively, within the film plane.

In order to generate hysteresis loops, one must make an assumption concerning the process of magnetization reversal in the sample. One might assume that the system always finds the absolute minimum energy state for a given value of the applied field. Alternatively, if we assume that the magnetization of each layer rotates coherently as a single domain, then the system passes through a series of local energy minima as the applied field is changed. A hysteresis loop may be easily generated by starting from the saturated state, where $\theta_1 = \theta_2 = \theta_H$ and decreasing the field value in small steps. Using the values of θ_1 and θ_2 from the previous step as starting values, a modified Newton algorithm is then used to compute the new values of θ_1 and θ_2 at the lower field value.[22] Having calculated the values of these angles as a function of the applied field strength, one may then plot M-H loops for the components of the magnetization both parallel and perpendicular to the applied field. K_i/M was iteratively varied in order to obtain the best fit for loops with the field aligned close to the hard axis ($\sim 2°$ misalignment between the field and the hard axis). Because we have assumed coherent rotation we only attempt to fit the M-H loops along the hard axis.

Calculations of the magnitude of the MOKE signal normalized to the saturation value were made by modeling the optical response of a stratified, multilayer system using a scattering matrix formalism[23] modified to include the effect of an applied dc magnetic field or magnetization.[24] The magnitude and orientations of the magnetiza-

tions were calculated using the minimum energy technique described above. Calculations for our samples indicated that the MOKE signal was proportional to the relevant component of the vector sum of the two Co-layer moments because the thicknesses of the layers were much less than the optical skin depth. Therefore the theoretical results for the magnetization components have been used as fits to the measured MOKE data.

Simulations of the Co/Cu/Co trilayer system indicated that it was possible to determine the coupling strength from the behavior of the $M_\perp$-H loop with the field applied close to the hard axis direction, but the $M_\parallel$-H loop was relatively insensitive to the magnitude of the coupling strength. This is illustrated in Fig. 2, which shows the M-H loops of this system for (a) $M_\parallel$ and no coupling, (b) $M_\parallel$ and small coupling where the coupling field ($8A_{12}/Md$) is 1% of the anisotropy field ($2K/M$), (c) $M_\perp$ and no coupling, and (d) $M_\perp$ and the small coupling as in (b). The $M_\parallel$-H loops show no obvious dependence on the coupling strength, whereas the $M_\perp$-H loop "collapses" as the coupling strength is increased. This collapse occurs within a well defined in-plane angular range centered around the sample's hard axis, with an angular width that also increases with coupling strength. In the example above a range of $\pm 0.1°$ is observed for the 1% coupling strength used. This effect is due to the competition between the AF coupling, which tends to keep the magnetizations in each layer apart, and the anisotropy, which tends to favor a parallel alignment of magnetizations. It is also possible to get a collapse in the $M_\perp$-H loop if the sample breaks down into regions of randomly oriented domains or if there is a small angular spread in the position of the hard anisotropy axis within the sample. Nonetheless, the angular width measurement provides an upper bound on the coupling strength of the sample.

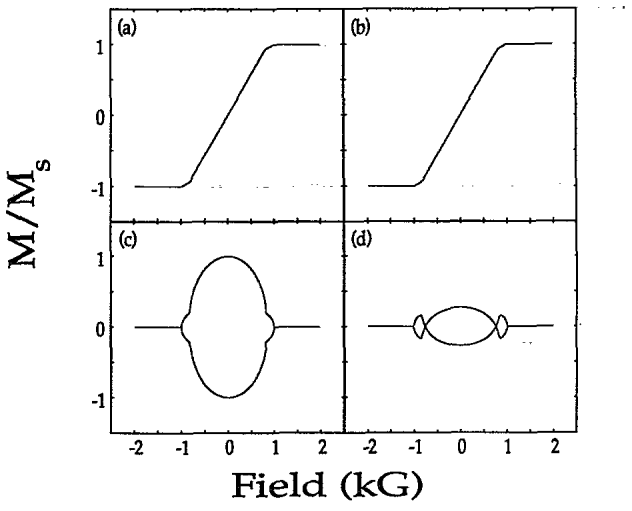

FIG. 2. Calculated M-H loops for a Co/Cu (20 Å)/Co system for two values of coupling strength. (a) $M_\parallel$ and no coupling; (b) $M_\parallel$ and small coupling; (c) $M_\perp$ and no coupling; (d) $M_\perp$ and small coupling.

B. Magnetic response of the samples

MOKE measurements of both samples produced similar results, and so only those for sample A will be discussed in detail here. Measurements of $M_\parallel$-H loops were first made in the LF/LM geometry on sample A. The easy and hard anisotropy axes of the sample were located by measuring a series of loops as the sample was rotated in-plane. They correspond to substrate crystallographic directions of $(1\bar{1}1)$ and $(1\bar{1}\bar{2})$, respectively. Figure 3 shows the resulting easy (a) and hard (b) loops. The anisotropy constants for each layer were derived from the experimental data using the fitting procedure described above and produced the values listed in Table II. These results indicate that only a strong uniaxial anisotropy is present, which is surprising, since the crystallographic structure of the sample, as determined by RHEED, should yield a uniaxial and fourfold anisotropy in the bottom bcc (110) Co layer (with the fourfold anisotropy dominant) and a weak sixfold anisotropy in the top fcc (111) Co layer. The magnitudes of the uniaxial anisotropies are large for both layers, but are comparable with previous results for epitaxial bcc (110) Co films,[18,19] and we therefore infer that the role of the crystallographic structure of the film is weak and that the uniaxial anisotropy is defect induced or strain induced and associated with the substrate.

The easy axis loop shows four levels [Fig. 3(a) (i), (ii), (iii), and (iv)] and is consistent with switching in which

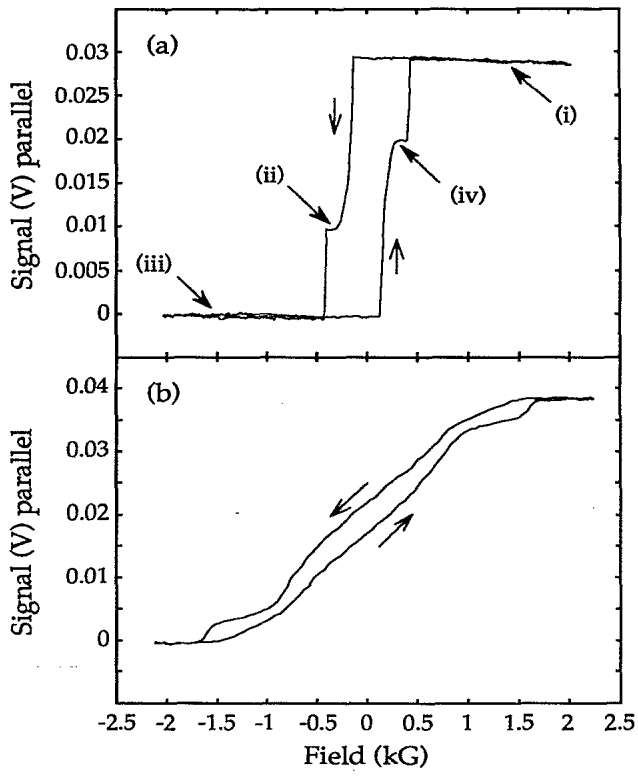

FIG. 3. The measured $M_\parallel$-H loops using the LF/LM geometry for easy (a) and hard (b) anisotropy axes lying parallel to the field.

TABLE II. The anisotropy constant (±10%) determined by fitting the calculated data to the experimental data for each sample.

	Sample A 27 Å Cu interlayer	Sample B 20 Å Cu interlayer
K_i for top Co layer	4.5×10^4 Jm^{-3}	5.7×10^4 Jm^{-3}
K_i for bottom Co layer	9.0×10^4 Jm^{-3}	7.0×10^4 Jm^{-3}

the remanent magnetization is due to parallel alignment of the two moments. In saturation [levels (i) and (iii)] the magnetizations in each layer are parallel to each other and to the applied field, while the intermediate levels [(ii) and (iv)] correspond to the magnetizations oriented antiparallel to each other but remaining parallel to the applied field. This behavior shows that any coupling if present is very weak compared to the anisotropy strength (since both the parallel and antiparallel states are destroyed by the application of small fields) and gives clear evidence of two separate magnetic layers indicating that pinholes are absent. An upper bound on the coupling strength was determined from the $M_\perp$-H loop as described in the previous section, and this result is discussed together with the $M_\perp$-H loops in Sec. IV C.

The relative magnitude of these levels is important in determining the total amount of magnetic material in each cobalt layer and can be related to the moments for each layer. They can also be used to determine which layer switches first. When the two Co layers have equal thicknesses and magnetizations, the two intermediate levels [(ii) and (iv)] should be almost equal, as shown by the calculation in Fig. 4(a). When there are unequal layer thicknesses or magnetizations then the relative positions of levels (ii) and (iv) will change, as indicated in Fig. 4(b), where a bottom layer half as thick as the top layer was used in the calculation. Therefore, by examining the relative positions of the corresponding measured levels it is possible to determine the ratio between the products of the thickness and magnetization for the two Co layers.

The measured loop [Fig. 3(a)] indicates that this ratio is not unity for this sample, and calculations show that the ratio of the moments of the top layer to bottom layer ~2 (a similar ratio was found for sample B). Polar

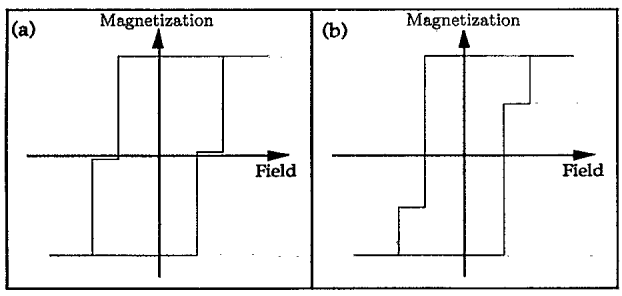

FIG. 4. A schematic showing how different Co layer thickness ratios can effect the easy axis $M_\parallel$-H loop. In (a) the ratio of the top Co layer to the bottom Co layer is 1:1; in (b) the ratio is 2:1. The top layer switches first.

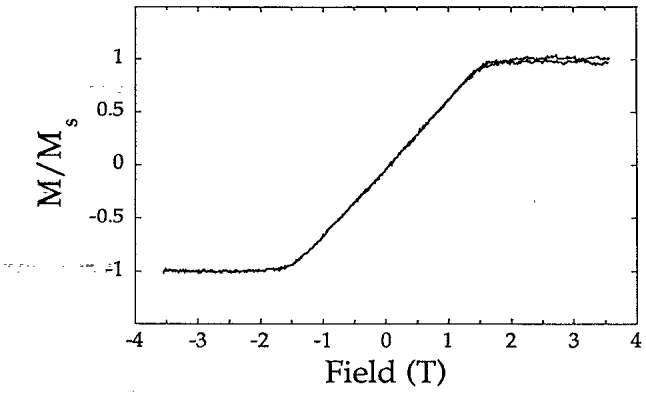

FIG. 5. The measured polar MOKE loop, which shows equal saturation fields for both Co layers (~1.8 T).

MOKE measurements made with a superconducting magnet (Fig. 5) indicate that both layers saturate at the same applied field value (~1.8 T) implying that the demagnetizing fields $\mu_0 M$ of each layer are approximately the same. Thus the difference in the magnetic moment ratio is only due to the difference in the thicknesses of the two Co layers. This result is confirmed by polarized neutron reflection (PNR) measurements,[25] which indicate both a thickness ratio of ~2, with the top layer having the larger thickness, and equal magnetizations in both Co layers. One explanation for this large ratio is that there has been some interdiffusion or chemical reaction at the Co/Ge interface which reduces the effective thickness of magnetic material in the bottom Co layer by ~15 Å. In support of this view, evidence for interdiffusion at the Co/Ge interace[26] and chemical reaction at the Fe/Ge interface[27] have been reported.

Since the top layer has a bigger moment than that of the bottom layer and a larger change occurs between levels (i) and (ii) than between levels (ii) and (iii) in Fig. 3(a) it is clear that the top layer switches first.

C. Evidence of magnetization rotation

MOKE measurements of $M_\perp$-H loops were made in the TF/LM geometry with the hard axis of the sample approximately 2° from the applied field, and are presented along with the $M_\parallel$-H loop and the corresponding theoretical calculations in Fig. 6 for sample A. The TF/LM and LF/LM results indicate that the full magnetization lies along the easy anisotropy axis for zero applied field, since the magnitude of the $M_\perp$-H loop in the TF/LM geometry at zero field is equal to that of the $M_\parallel$-H loop in the LF/LM geometry when the sample is saturated. From this observation it is clear that a coherent rotation of the magnetizations in each layer has occurred as the field is varied along the hard anisotropy axis of the sample.

The fit between the theoretical and the measured results is good, indicating that coherent magnetization rotation actually occurs in the sample. The fits also indicate that there is no significant coupling between the two magnetic layers in this sample (and similarly for sample B). The coupling strength can be given an upper bound by measuring the collapse in the $M_\perp$-H loop close to the

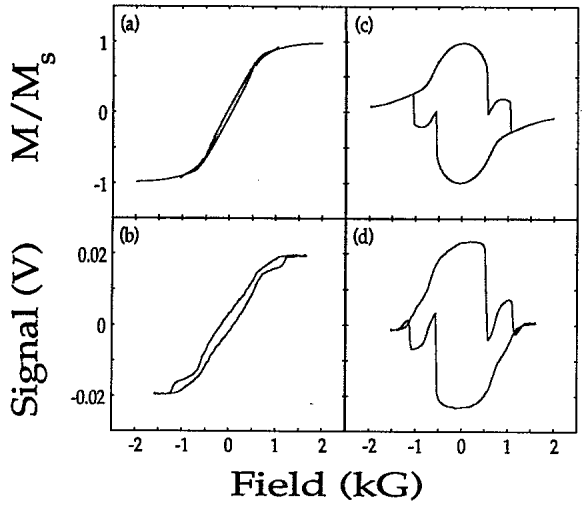

FIG. 6. A comparison of the calculated $M_{\parallel}$-H (a) and $M_{\perp}$-H (c) loops, and the measured $M_{\parallel}$-H (b) and $M_{\perp}$-H (d) loops for the Co/Cu (27 Å)/Co sample described in the text.

hard axis. An angular spread of $\pm 0.1°$ was observed for this effect, and simulations fit this spread for a coupling strength $\sim 1\%$ of the anisotropy strength. This is surprising, since previous work on *sputtered* samples has suggested that there is FM and AF coupling at the two interlayer thicknesses of 27 and 20 Å, respectively, used in our samples.[7] However, recent results[11–14] have shown the importance of the structural integrity of MBE-grown samples with regard to the observation of coupling in such structures. We attribute the absence of coupling to the increased interface roughness of our samples in comparison with similar samples grown on an Au seed layer.[13]

It is remarkable that at zero applied field, there is a uniform parallel alignment of magnetizations corresponding to the full saturation values. This implies that the laser spot is probing a single domain or the entire sample is switching as a single domain. While domain microscopy is required to unambiguously confirm this, we do observe the same behavior wherever the laser spot is positioned on the sample, suggesting that the entire sample is indeed single domain. Furthermore the beam diameter (~ 2 mm) is large on the scale of *bulk* magnetic domains in Co, though large domains are seen for ultrathin Co/Cu films.[21] It should also be noted that the PNR measurements are made over the whole sample area and give results that are consistent with this finding.

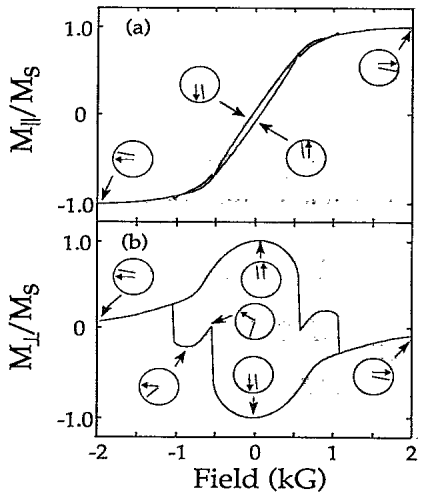

FIG. 7. The calculated $M_{\parallel}$-H (a) and $M_{\perp}$-H (b) loops for the Co/Cu (27 Å)/Co system described in the text, showing the directions of the magnetizations at various points on the loops as indicated by the insets.

It is possible to plot out the orientations of the magnetizations from the theoretical results and examine how they contribute to each loop. This is shown in Fig. 7, which shows the calculated $M_{\parallel}$-H and $M_{\perp}$-H loops with insets indicating the orientations of the two magnetization components for various points on the curves. In the insets the field direction is horizontal, the line with the arrow corresponds to the magnetization of the top layer, while the plain line corresponds to the magnetization of the bottom layer. The nature of the sample's switching behavior can thus be determined with reference to these diagrams. In particular it can be seen that the sharp features occurring at fields of ± 0.5 and ± 1 kG are associated with an abrupt transition in which the magnetizations in the top and bottom Co layers, respectively "flip" over their own hard axis. From this it can be seen that measurements of $M_{\perp}$-H loops for switching in the vicinity of the hard axis provide a sensitive means of determining the layer-dependent anisotropy fields K_i/M.

V. CONCLUSIONS

We have shown how it is possible to observe the magnetization reversal process by measuring the magnitudes of the two components of magnetization parallel and perpendicular to the applied field in the plane of the sample directly as a function of the saturation value. This is accomplished by using two MOKE geometries in which the applied field is rotated through 90°, rather than by changing the analyzer setting. We show that the parallel M-H loop near to the hard axis is insensitive to the ratio of a weak-coupling field to the anisotropy field, whereas the perpendicular M-H loop shows a strong dependence on this ratio. This finding demonstrates the usefulness of studying the vectorial magnetization process.

A Co/Cu(111)/Co trilayer system was used to illustrate this procedure and the results indicated that the full magnetizations of each layer were aligned along the easy anisotropy axis when the applied field along the hard anisotropy axis was decreased from its saturation value to zero. The magnetization reversal proceeds by coherent rotation of the bulk magnetization vector. Calculations based on an energy minimization technique provided a good fit to the experimental data and enabled fits for the anisotropy constants of each layer to be accurately obtained. The strong uniaxial anisotropies observed are not consistent with the crystallographic structure as determined by RHEED, suggesting that strain or defects may dominate the anisotropy behavior.

The Cu interlayer thicknesses for the MBE-grown samples were chosen to correspond to thicknesses at which FM and AF coupling has been observed in similar sputtered samples. However, no significant coupling was observed in either sample.

ACKNOWLEDGMENTS

The financial support of the SERC, the Toshiba Corporation, and the Newton Trust, Cambridge for this work is gratefully acknowledged.

[1]U. Admon, M. P. Dariel, E. Grunbaum, and J. C. Lodder, J. Appl. Phys. **66**, 316 (1989).
[2]J. M. Florczak and E. Dan Dahlberg, J. Appl. Phys. **67**, 7520 (1990).
[3]J. M. Florczak and E. D. Dahlberg, Phys. Rev. B **44**, 9338 (1991).
[4]Q. M. Zhong, A. S. Arrott, B. Heinrich, and Z. Celinski, J. Magn. Magn. Mater. **104**, 1837 (1992).
[5]S. S. P. Parkin, N. More, and K. P. Roche, Phys. Rev. Lett. **64**, 2304 (1990).
[6]M. N. Baibich, J. M. Broto, A. Fert, F. Nguyen Van Dau, P. Etienne, G. Creuzet, A. Friedrich, and J. Chazelas, Phys. Rev. Lett. **61**, 2472 (1988).
[7]S. S. P. Parkin, R. Bhadra, and K. P. Rocher, Phys. Rev. Lett. **66**, 2152 (1991).
[8]B. Dieny, V. S. Speriousu, B. A. Gurney, S. S. P. Parkin, D. R. Wilhoit, K. P. Roche, S. Metin, D. T. Peterson, and S. Nadimi, J. Magn. Magn. Mater. **93**, 101 (1991).
[9]D. M. Edwards, J. Mathon, R. B. Muniz, and M. S. Phan, Phys. Rev. Lett. **67**, 493 (1991).
[10]R. Coehorn, Phys. Rev. B **44**, 9331 (1991).
[11]W. F. Egelhoff, Jr. and M. T. Kief, Phys. Rev. B **45**, 7795 (1992).
[12]M. T. Johnson, R. Coehorn, J. J. de Vries, N. W. E. McGee, J. aan de Stegge, and P. J. H. Bloemen, Phys. Rev. Lett. **69**, 969 (1992).
[13]D. Greig, J. J. Hall, C. Hammond, B. J. Hickey, H. P. Ho, M. Howson, M. J. Walker, N. Wiser, and D. G. Wright, J. Magn. Magn. Mater. **110**, L239 (1992).
[14]A. Schreyer *et al.* (unpublished).
[15]J. A. C. Bland, M. J. Padgett, R. J. Butcher, and N. Bett, J. Phys. E **22**, 308 (1989).
[16]M. Rührig, R. Schäfer, A. Hubert, R. Mosler, J. A. Wolf, S. Demokritov, and P. Grünberg, Phys. Status Solidi A **125**, 635 (1991).
[17]J. C. Slonczewski, Phys. Rev. Lett. **67**, 3172 (1991).
[18]G. A. Prinz, Phys. Rev. Lett. **54**, 1051 (1985).
[19]G. A. Prinz, C. Vittoria, J. J. Krebs, and K. B. Hathaway, J. Appl. Phys. **57**, 3672 (1985).
[20]J. Chen and J. L. Erksine, Phys. Rev. Lett. **68**, 1212 (1992).
[21]A. Berger, U. Linke, and H. P. Oepen, Phys. Rev. Lett. **68**, 839 (1992).
[22]P. Dieny, J. P. Gavigan, and J. P. Rebouillat, J. Phys.: Condens. Matter **2**, 159 (1990).
[23]D. Y. K. Ko and J. R. Sambles, J. Opt. Soc. Am. A **5**, 1863 (1989).
[24]C. Daboo and H. P. Hughes (private communication).
[25]J. A. C. Bland, *et al.* (unpublished).
[26]M. Genut and M. Eizenberg, J. Appl. Phys. **68**, 2146 (1990).
[27]W. Folkerts, W. Hoving, and W. Coene, J. Appl. Phys. **71**, 362 (1992).